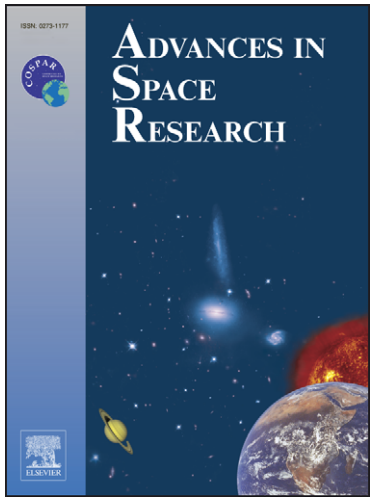

A polytropic model for the solar wind

C. Jacobs, S. Poedts

PII: S0273-1177(11)00589-8
DOI: 10.1016/j.asr.2011.08.015
Reference: JASR 10695

To appear in: *Advances in Space Research*

Received Date: 13 April 2010
Revised Date: 5 August 2011
Accepted Date: 12 August 2011

Please cite this article as: Jacobs, C., Poedts, S., A polytropic model for the solar wind, *Advances in Space Research* (2011), doi: 10.1016/j.asr.2011.08.015

A polytropic model for the solar wind

C. Jacobs[a,b], S. Poedts[a,b]

[a] *Centrum voor Plasma-Astrofysica, Celestijnenlaan 200B, 3001 Leuven, Belgium*
[b] *Leuven Mathematical Modeling and Computational Science Centre, Leuven, Belgium*

Abstract

The solar wind fills the heliosphere and is the background medium in which coronal mass ejections propagate. A realistic modelling of the solar wind is therefore essential for space weather research and for reliable predictions. Although the solar wind is highly anisotropic, **magnetohydrodynamic** (MHD) models are able to reproduce the global, average solar wind characteristics rather well. The modern computer power makes it possible **to perform full three dimensional (3D) simulations in domains extending beyond the Earth's orbit**, to include observationally driven boundary conditions, and to implement even more realistic physics in the equations. In general, **MHD models for the solar wind often make use of additional source and sink terms in order to mimic the observed solar wind parameters and/or they hide the not-explicitly modelled physical processes in a reduced or variable adiabatic index.** Even the models that try to take as much as possible physics into account, still need additional source terms and fine tuning of the parameters in order to produce realistic results. In this paper we present a **new and simple** polytropic model for the solar wind**, incorporating data from the ACE spacecraft to set the model parameters. This approach allows to reproduce the different types of solar wind**, where the simulated plasma variables are in good correspondence with the observed solar wind plasma near 1AU.

Keywords: Solar wind, magnetohydrodynamics, numerical modelling

1. Introduction

The Sun's outer atmosphere is so hot that gravity cannot prevent it from continuously expanding. The continuous stream of high energetic particles emanating from

Email addresses: Carla.Jacobs@wis.kuleuven.be (C. Jacobs), Stefaan.Poedts@wis.kuleuven.be (S. Poedts)

the Sun is known as the *solar wind*. Parker (1958) was the first to realise that the solar corona has to expand and he predicted a transonic outflow from the hot corona into interplanetary space. **Shortly after** the first detections of a supersonic flow in interplanetary space were made by a group of Russian scientists **during the Luna 1 mission in 1959**. The unequivocal existence of the solar wind was established by the Mariner 2 spacecraft launched in 1962, when it became immersed in a continuous flow once it crossed the Earth's magnetopause.

The bulk of the solar wind consists of electrons and protons. The next most abundant ion is He^{2+}. Also traces of heavier ions in different ionisation stages are present. In fact, the composition of the solar wind reflects the chemical composition of the solar atmosphere. Space missions have revealed the existence of different types of solar wind. The source regions and the properties of the different types of solar wind are summarized by, for example, Schwenn (2006). There are two main types of solar wind: a fast, tenuous, and almost uniform stream, and a slow, dense component. The sources of the fast solar wind are the regions in the corona of "open" magnetic field or coronal holes. The fast solar wind is originating from the inactive, quiet part of the Sun. The slow wind is more turbulent than the fast wind and originates from the tips and edges of temporarily open streamers or from opening loops and active regions. **The helium abundance in the slow solar wind increases from** $< 2\%$ **during minimum to around** 4% **at times of solar maximum, indicating that the morphology of the source regions of the slow solar wind are changing over the course of the solar cycle (Schwenn 2006).**

The main difference between the fast and slow solar wind is the flow velocity. Using interplanetary scintillation, Breen et al. (2002) demonstrated that there is a difference in acceleration between the fast and slow wind. The main acceleration of the fast solar wind happens low in the solar corona, with 50% of the asymptotic speed reached by 4-5 $R_\odot$. The fast wind is accelerated almost to its final flow velocity within 20 $R_\odot$ and a small but not neglegible acceleration exists beyond 30 $R_\odot$ (Kojima et al. 2004). In interplanetary space the fast wind has speeds exceeding 700 km s^{-1}. The acceleration of the slow solar wind is starting at higher radial distances than for the fast wind and is more gradual. Most of the slow acceleration seems to take place between 5 and 10 $R_\odot$, but the slow wind continues to accelerate out to 25-35 $R_\odot$ and its velocity is only around 300 km s^{-1}, on average.

Spacecraft like the Advanced Composition Explorer (ACE) are continuously measuring the solar wind properties near the Earth. From satellite observations it is known that at the Earth the solar wind is highly variable. It can be as slow as 250 km s^{-1} and faster than 750 km s^{-1}, but typically it has a velocity of about 400 km s^{-1}. The density in the solar wind is more variable than the velocity, ranging from about 0.1 cm^{-3} to 100 cm^{-3}. The Ulysses spacecraft, **that was flying in a solar polar orbit between 1990 and 2009**, has provided scientists for the first time with direct measurements of the solar wind plasma and magnetic field at high-latitude positions. **During its operational time, the spacecraft completed almost three full orbits around the Sun and** almost two solar cycles of measurements are available, **which led us learn** that the variation in solar wind properties changes with latitude during the course of the solar cycle, in close correspondence with the changes in the source regions of the solar wind in the lower corona (McComas et al. 2003, 2008). During solar minimum the fast wind dominates the heliosphere from about 20° above and below the equatorial plane, whereas during solar maximum a more complex pattern of alternating slow and fast wind is observed. The heliocentric distance of the Ulysses spacecraft varied between 1.3AU and 5.4AU and it scanned the heliolatitudes between ±80.2°. The unique orbit of the Ulysses spacecraft makes it possible to quantify the radial and latitudinal variances in the solar wind, as has recently been published by Ebert et al. (2009). Their main conclusions were: 1) the proton temperature in the slow wind falls less rapidly with distance than in the fast wind; 2) the total interplanetary magnetic field (IMF) strength drops **slower** with distance in the slow wind than in the fast wind, due to the tighter Parker spiral structure in the slow wind; 3) the latitudinal variations are small, both for the slow and fast wind. The first conclusion of Ebert et al. (2009) is in contradiction with the specifications in Schwenn (2006). This might be due to the fact that 1) the observations used in Schwenn (2006) were limited to the ecliptic plane (Helios and ACE data); 2) Ebert et al. (2009) did not distinguish between the two types of slow solar wind; or 3) the radial dependence of the solar wind plasma is different for large distances (>1AU) (other physical processes, like the effect of pickup ions, are becoming important at larger heliocentric distances).

Numerical simulations of the solar wind are complementary to the observations and necessary to develop a better understanding of the effect of the solar wind on the propagation of interplanetary shocks and magnetic clouds. A realistic, time-dependent

modelling of the solar wind is therefore essential for space weather modelling and forecasting. Among the most important unanswered questions in solar physics are: what are the mechanisms causing the heating of the solar corona to its million degree temperature and what are the mechanisms accelerating the solar wind to its superfast **speed**? **Wave energy has been suggested as a possible driving mechanism for the solar wind since a long time (e.g. Hollweg 1986). Recent observations prove that Alfvén waves are the likely source of energy that drives the solar wind (McIntosh et al. 2011). The wave pressure provides acceleration of the solar wind, while their gradual dissipation causes heating of the plasma. A review of wave driven solar wind models is found in Ofman (2010). Close to the solar surface, radiative cooling and thermal conduction play an important role as well.** From observations it is clear that the solar wind **temperature** is highly anisotropic with respect to the magnetic field vector, electrons and ions are not in thermal equilibrium, and the plasma is almost collisionless. This **means** that, theoretically, the classic model of magnetohydrodynamics (MHD) is not applicable for solar wind modelling. However, full three dimensional (3D) kinetic modelling is still out of scope due to the high level of complexity of the problem and the enormous amount of computer resources needed. Therefore, MHD models for the solar corona are fairly popular, despite **their** shortcomings, and are able to reproduce the global structure of the solar wind rather well (Parker 2007). **One of the most sophisticated models currently available in the literature is the two-temperature model of van der Holst et al. (2010). This 3D model considers the protons and electrons to have different temperatures, it includes anisotropic thermal heat conduction for the electrons, Alfvén waves to heat and accelerate the protons, and it uses data-driven boundary conditions for the coronal magnetic field, density, and temperature.** Because of the increased computer power during the last decade, 3D modelling of the solar wind is becoming more and more the standard (e.g Linker et al. 1999; Roussev et al. 2003; Hayashi et al. 2006; Usmanov and Goldstein 2006; Cohen et al. 2007; Nakamizo et al. 2009). The current solar wind models differ in the physics included in the equations and the treatment of the source terms. The unknown physics is often counterbalanced by the inclusion of additional source terms with some ad hoc description. In order to obtain realistic results, comparable to the observations at 1AU, a long process of deriving suitable values for the free parameters in the model often precedes. In general, two main classes of MHD solar wind

models can be distinguished: **models adding extra source terms to the energy and momentum equations of the classic MHD system to represent the missing physics, and the models using a reduced/variable adiabatic index. A subset of the latter are the polytropic models, which explicitly assume a relation of the form $p \sim \rho^{\alpha}$ between the pressure, p, and the density, ρ. The polytropic index is often assumed close to unity in order to represent the nearly isothermal corona of the Sun and to obtain the acceleration of the solar wind. A recent observationally based estimate of the effective adiabatic index in the solar corona by Van Doorsselaere et al. (2011) yields a value of $\gamma = 1.1 \pm 0.02$. Since the relation between the pressure and the density is explicitly known under the polytropic assumption, the energy equation can be omitted, simplifying the set of equations to solve. In this paper a model for the solar wind is presented, that starts from the polytropic assumption and that includes the observational data of the solar wind plasma near 1AU. A detailed description of this new approach for a polytropic model is described in Sect. 2. The results of our model runs are presented in Section 3.** We end this paper with a concluding Section 4.

2. A new polytropic model for the solar wind

In astrophysics, a polytropic relation between the pressure p and density ρ (i.e. $p \sim \rho^{\alpha}$) is commonly used. A well known example is the Lane-Emden equation, describing the mass and pressure inside a star (Chandrasekhar 1939). By considering a polytropic relation between pressure and density, the energy equation can be omitted from the set of equations to solve. This approach is used in many numerical studies of the solar wind and **propagation of coronal mass ejections (CMEs)** (e.g. Linker and Mikić (1995); Linker et al. (2003); Riley et al. (2006), but also Wang et al. (1995); Wu et al. (1999); Keppens and Goedbloed (1999, 2000); Hu et al. (2008)). Such simplified polytropic models yield surprisingly good approximations and can reproduce many qualitative features of the observed solar corona **(Hayashi et al. 2006)**. Because of its simplicity, the polytropic wind model is still fairly popular, in spite of its clear shortcomings. This kind of wind model is for example not able to reproduce the fast solar wind speed in regions of open magnetic field. This artifact is the result of assuming both polytropic and adiabatic flow, and as such isentropic flow.

To derive the ideal MHD equations, the ideal gas assumptions are explicitly used.

In an ideal gas the internal energy is assumed to be solely dependent on the temperature, and the ratio of the specific heats $\gamma = c_p/c_v$ is assumed to be constant. In case of an adiabatic process, the relation

$$\frac{Dp}{Dt} - \frac{\gamma p}{\rho}\frac{D\rho}{Dt} = 0$$

between the pressure and density holds, yielding

$$\frac{D}{Dt}\frac{p}{\rho^\gamma} = 0,$$

where the quantity p/ρ^γ is associated with the entropy, S, of the gas. **Under the polytropic assumption $p \sim \rho^\alpha$ the process is adiabatic only if the polytropic index α satisfies the relation**

$$\alpha = \left.\frac{\partial \ln p}{\partial \ln \rho}\right|_S .$$

However, whenever this condition is not satisfied it can be derived that:

$$\frac{Dp}{Dt} - \frac{\gamma p}{\rho}\frac{D\rho}{Dt} = (\gamma - \alpha)p\nabla \cdot \mathbf{v},$$

where $\mathbf{v}$ is the velocity vector. This is equivalent to assuming that the process is not adiabatic. In case of expansion of the medium, like in the solar corona, extra heat will be added to the system when $\alpha < \gamma$. From measurements it is established that the temperature of the solar wind plasma decreases with radial distance from the Sun, but it does not cool rapidly enough to be considered as adiabatic expansion (Goldstein et al. 1996). Assuming a polytropic relation for the solar wind plasma and that the matter has three degrees of freedom, leads to: $1 < \alpha < 5/3 = \gamma$. A polytropic behaviour of the solar wind was identified by Totten et al. (1995). These authors concluded from the analysis of Helios 1 data that the solar wind behaved fairly polytropic between 0.3 AU and 1 AU, with $\alpha = 1.46$ as an average value for the polytropic index and that the polytropic index was rather independent of the solar wind type.

In the next subsection we describe how, by using the more general polytropic relation mentioned above, the two components of solar wind can easily be reproduced.

2.1. Description of the model

In the classic MHD model it is assumed that the number of protons and electrons is equal, $n_p = n_e = n/2$, and that they are in thermal equilibrium, $T_p = T_e = T$. In the general case of polytropic flow the relation between pressure and density reads

$$p = Kn^\alpha,$$

where n is the total particle density ($n = n_p + n_e$) and the parameters K and α are **constants**. Combining the polytropic relation with the ideal gas law, we obtain

$$K = k_B T n^{1-\alpha},$$

with k_B the Boltzmann constant.

Using the above considerations, it is clear that the polytropic relation derived by Totten et al. (1995) cannot hold **true** all the way to the lower solar corona. This can be **demonstrated** by a simple example. Taking typical values of the fast solar wind at 1AU, $n_p = 2\,\mathrm{cm}^{-3}$, $T_p = 2.5 \times 10^5\,\mathrm{K}$ and $\alpha = 1.46$, we obtain a value of $K = 3.2 \times 10^{-21}\,\mathrm{N\,m}^{3\alpha-2}$. Holding the value of K and α constant, and taking a typical coronal hole density of $1 \times 10^8\,\mathrm{cm}^{-3}$, a temperature of $8.7 \times 10^8\,\mathrm{K}$ is obtained! Near the solar surface, the solar wind is assumed to be nearly isothermal and a value of the polytropic index closer to one might be more appropriate. Using the same example as above, but reducing α to a value of $\alpha = 1.25$ yields a more realistic coronal temperature **at the base** of $8.6 \times 10^5\,\mathrm{K}$. **In case the observational value of** $\alpha = 1.1$ **measured by Van Doorsselaere et al. (2011) is used, the factor** K **has to be increased to a value of** $K = 4.4 \times 10^{-19}\,\mathbf{N\,m}^{3\alpha-2}$ **in order to get the same value for the coronal temperature. In the model presented in this paper the classic polytropic assumption is modified and the parameters** α **and** K **are allowed to vary in space. This yields that energy will not be conserved in this model.**

When calculating the gradient of the pressure, it is evident that including spatial variation in the parameters K and α will have an effect on the acceleration of the solar wind:

$$\nabla p = K n^{\alpha} \alpha \frac{\nabla n}{n} + K n^{\alpha} \left(\frac{\nabla K}{K} + \ln(n) \nabla \alpha \right). \tag{1}$$

We can consider the following two special cases:

Isothermal flow. In this case $\gamma = \alpha = 1$. The temperature is constant at all time, and so $K = k_B T_0$ is constant. The flow is by definition isentropic and and the gradient in pressure reduces to:

$$\nabla p = k_B T_0 \nabla n.$$

Isentropic flow. In the case of isentropic flow, it is assumed that p/ρ^{γ} is constant, in other words, $K = K_0$ and $\alpha = \gamma$ both constant. Under these conditions, the expression

for the pressure gradient is given by:

$$\nabla p = K_0 n^\alpha \alpha \frac{\nabla n}{n}.$$

For a value of $\alpha > 1$ this has a reducing effect on the pressure gradient, and as such on the acceleration of the flow. This is easy to see when assuming for example $n \sim r^{-2}$. Even for a small value of $\alpha = 1.05$, the isentropic flow deviates already strongly from the isothermal flow, having a much lower asymptotic wind speed. The higher the value of the polytropic index, the slower the flow (see for example Keppens and Goedbloed 1999). In the general polytropic case, where both K and α can be position dependent, the final flow profile will be strongly dependent on the spatial variation of both parameters. **The mechanisms that accelerate the solar wind to its superfast velocity are not explicitly modelled in this way, but hidden in the varying parameters α and K.**

Since the acceleration profile is different in the two types of solar wind (see introduction), it is natural to assume a different radial variation of the polytropic parameters in the two solar wind types. The results presented in the next subsection were all obtained with a spatial variation for the parameters α and K of the following form:

$$\alpha(r) = \begin{cases} \alpha_0, & \text{if } r < r_1, \\ \alpha_0 + (\alpha_1 - \alpha_0)\sin^2\left(\frac{\pi}{2}\frac{r-r_1}{r_2-r_1}\right), & \text{if } r_1 \le r \le r_2, \\ \alpha_1, & \text{if } r > r_2, \end{cases}$$

The value of α is smoothly varying between the value α_0 close to the Sun and its value near 1AU, α_1**, where the variation in α takes place between the radial distances r_1 and r_2.** The functional form of the factor $K(r)$ is chosen accordingly to

$$K(r) = K_0 n_0^{\alpha_0 - \alpha(r)} f(r),$$

where

$$f(r) = \begin{cases} 1, & \text{if } r < r_1, \\ 1 + (K_1 - 1)\sin^2\left(\frac{\pi}{2}\frac{r-r_1}{r_2-r_1}\right), & \text{if } r_1 \le r \le r_2, \\ K_1, & \text{if } r > r_2, \end{cases}$$

with $K_1 = K_{1\mathrm{AU}}/K_0 n_0^{\alpha_0 - \alpha_1}$. The value of $K_{1\mathrm{AU}}$ can be chosen from Table 3 in Totten et al. (1995). **Beyond a distance of r_2 the parameters K and α remain constant and the solution is described by a real polytrope.** By choosing the coronal density

n_0, temperature T_0, and polytropic index α_0 the value of K_0 can be fixed. Fludra et al. (1999) have investigated the density and the temperature of the lower solar corona. In their observations they found that the density and the temperature in the coronal holes is lower than in the closed field regions. As a value for the electron density near the limb they found $5 \times 10^8\,\mathrm{cm}^{-3}$ in the equatorial region and $2 \times 10^8\,\mathrm{cm}^{-3}$ in the polar regions. The temperature near the limb varied between $7 \times 10^5\,\mathrm{K}$ (polar region) to $1.1 \times 10^6\,\mathrm{K}$ (equator) and away from the solar limb the temperature was increasing. A realistic model for the solar corona must include this non-uniform temperature and density distribution over the solar surface.

3. Results

In order to find out the model parameters that result in a realistic reconstruction of the solar wind, a series of 1.5D tests were performed. With 1.5D we mean that the assumptions are similar as in the Weber-Davis wind model (Weber and Davis 1967), namely $\frac{\partial}{\partial\theta} = \frac{\partial}{\partial\varphi} = 0$ and $v_\theta = B_\theta = 0$. The ideal MHD equations are solved with the Versatile Advection Code (VAC, Tóth 1996) on a non-equidistant mesh of 1200 grid points spanning the range $[1.03, 220]R_\odot$.

The desired solar wind properties at 1AU were set by looking at 10 years of ACE observations. In Fig. 1 scatter plots are shown of the daily averaged data measured by the SWEPAM instrument on board of the ACE satellite. A clear correlation exists between the velocity and the proton temperature, but for the density and magnetic field strength a large scatter is present in the data. However, the general trend is the faster the wind, the lower the density and the stronger the IMF. Linear regression is used to derive a relation between the solar wind velocity and the temperature (density). It should be noted that **interplanetary CMEs**, magnetic clouds and **corotating interaction regions (CIRs)** are not filtered out of the data. This relation serves only to set a rough estimate for the solar wind variables at 1AU in different conditions.

From the linear fit of the ACE data, for each velocity (v_∞) a corresponding density ($n_{1\mathrm{AU}}$) and temperature ($T_{1\mathrm{AU}}$) can be estimated, and as such a value for $K_{1\mathrm{AU}}$ can be derived:

$$K_{1AU} = k_b T_{1\mathrm{AU}} n_{1\mathrm{AU}}^{1-\alpha_1}.$$

From the 1.5D tests, it was found that a value of $\alpha_1 = 1.42$ gives the best results. This value is at the lower boundary of the value of the polytropic index as estimated

by Totten et al. (1995). The other free parameters in the model (α_0, r_1, and r_2) **were** chosen in order to reproduce as good as possible the estimated solar wind variables at 1AU and this with realistic values for the coronal density, n_0, and temperature, T_0. In Table 1 an overview is given of the model parameters used to obtain the best fit for each specific solar wind type. The first three rows in Table 1 show the pre-set solar wind velocity and corresponding proton density and temperature as derived from the ACE observations. The next seven rows contain the model parameters K_{1AU}, α_0, α_1, r_1, and r_2, and the values chosen for the coronal density and temperature (n_0, T_0). The last three rows represent the simulated values for the flow velocity, the proton density, and the temperature at 1AU. Figure 2 shows the radial variation of the solar wind velocity, the density, and the temperature for the different simulations listed in Table 1. Only for the very slow wind ($v_\infty = 300\text{kms}^{-1}$) it turned out to be necessary to increase the value of the polytropic index from $\alpha_1 = 1.42$ to $\alpha_1 = 1.46$. The value of α_0 is depending on the type of solar wind flow, as well as the range $[r_1, r_2]$ whereover the variation in α and K takes place. This range is taken longer for the slower wind, since it is observationally known that the acceleration of the slow wind takes place over a larger spatial interval.

3.1. Extension of the model to 2.5D

The results from the 1.5D wind models are used to construct an approximation for the solar wind under solar minimum conditions. In the 2.5D model, the velocity and magnetic field vector are allowed to have all three components different from zero, but there is no variation in the azimuthal direction. The MHD equations are solved in spherical geometry on a grid containing 1200×91 cells, covering a full meridional plane, i.e. $(r, \theta) \in [1.03, 220]R_\odot \times [0, \pi]$, where θ is the co-latitude. In the 1.5D case it was trivial to keep the magnetic field divergence-free. In the 2.5D simulation the solenoidal condition is guaranteed by a similar approach as the constraint transport method of Evans and Hawley (1988).

The asymptotic solar wind speed is set accordingly to fit the Ulysses observations of the solar wind during minimum conditions: in a region of ±20° around the solar equator, the desired value for the solar wind velocity, v_∞, is chosen $400\,\text{km}\,\text{s}^{-1}$ and outside this region it is set to $750\,\text{km}\,\text{s}^{-1}$. Between the two regions of fast and slow solar wind we have a small transition region of 5° in which the asymptotic solar wind speed is changing linearly with latitude. In this simulation the solar wind flow is assumed to be independent of the azimuthal direction. Once the desired velocity at 1AU is specified

for each latitude, the density and the temperature are estimated from 10 years of ACE data, as mentioned above (Fig. 1). The value of the polytropic index at 1AU is set to $\alpha_1 = 1.42$. With all these variables defined, a value of the factor $K_{1\mathrm{AU}}$ can be obtained for each latitude. The polytropic parameters α and K are assumed to vary with radial distance in the same way as specified in Section 2.1. At the solar surface the value for the density, n_{base}, the temperature, T_{base}, and α_0 are set in correspondence with the 1.5D results. This yields a non-uniform density and temperature distribution at the inner boundary with a total particle density varying between $7 \times 10^8 \mathrm{cm}^{-3}$ at the equator and $3 \times 10^8 \mathrm{cm}^{-3}$ at the poles. The temperature increases from 1.25×10^6K in the polar areas to 1.62×10^6K in the equatorial region. The value of the polytropic index near the solar surface varies between the value $\alpha_0 = 1.30$ in the fast wind ($V_\infty > 600 \mathrm{km\,s}^{-1}$) and $\alpha_0 = 1.20$ in the slow wind ($V_\infty \leq 350 \mathrm{km\,s}^{-1}$). In this simulation, the global solar magnetic field is assumed to be a simple dipole with a field strength of 5 G at the poles. In the 1.5D simulations, the influence of the magnetic field strength on the acceleration of the flow is neglegible. In the 2.5D simulations, however, the Lorentz force is important and especially in the polar regions, the magnetic pressure causes additional acceleration of the flow, compared to the 1.5D test cases. Therefore, an additional correction is applied on the surface temperature, in order to obtain reasonable wind speeds near 1AU:

$$\tilde{T}_{\mathrm{base}} = T_{\mathrm{base}} + \left(T_{\mathrm{pole}} - T_{\mathrm{base}}\right) \cos\left(\frac{\pi}{2} \frac{\pi/2 - |\lambda|}{\pi/2 - \lambda_0}\right)^2 ,$$

when the absolute latitude, λ, becomes larger than λ_0 and T_{base} remains unmodified otherwise. Here we have chosen λ_0 equal to 65° and $T_{\mathrm{pole}} = 1.1 \times 10^6$K. **The lower polar temperature, compared to the 1.5D case, reduces the thermal pressure gradient, counterbalancing the additional acceleration due to the magnetic pressure and as such avoiding a too high coronal flow speed.**

A contour plot of the radial velocity is presented in Fig. 3. The figure also shows the magnetic field lines and zooms in on the region within $30R_\odot$ from the solar disk. Figure 4 shows the angular variation in the simulated solar wind velocity, the temperature, and the proton density at different radial distances. The bimodal solar wind structure is well represented and the solar wind variables have values in the range of the observations. Table 2 lists the values of the solar wind variables at the pole and the equator and this for two radial distances of 0.3AU and 1AU. The simulated solar wind data at 0.3AU are comparable with the measurements made by the Helios spacecraft.

4. Summary and conclusions

We have presented a new approach for the frequently employed polytropic model, used to simulate the solar wind flow. Polytropic models remain popular in solar wind modelling because they are easy to implement and can reproduce the typical white light characteristics of the solar corona. When focussing on the modelling of the solar corona, a constant polytropic index close to unity is usually considered. However, those models are unable to reproduce the bimodal wind structure and they cannot be extended all the way up to the Earth's orbit; the typical observed plasma values and power law dependencies cannot be reproduced when assuming a constant polytropic index. To overcome this problem, we have developed a polytropic wind model in which the model parameters are variable in space. **We have scanned the parameter space in order to find those values that provide the best fit of some typical solar wind values as derived from ACE data and that still fit within the observational constraints.** The variable model parameters represent the changing conditions in the physics driving the solar wind throughout the heliosphere. Therefore, different types of solar wind ask for a different functional representation of the model parameters. **In fact, this modelling approach is similar to including some ad hoc sink and source terms in the energy and momentum equations. Another well known model using a variable effective adiabatic index is the model of Roussev et al. (2003), later modified by Cohen et al. (2007). It has been demonstrated that this model is capable of reproducing the magnitude of the solar wind plasma variables rather well under solar minimum conditions (Cohen et al. 2008). A form of total energy is conserved in their model. The reduced adiabatic index results in a correction on the thermal pressure, which is similar in our model. However, the model presented here does not guarantee energy conservation.**

Models for the solar wind that are fast and accurate are important for space weather prediction. During the last decade, considerable progress has been made in the 3D MHD modelling of the solar corona, the propagation of solar transients through the heliosphere, and their interaction with the Earth magnetosphere (e.g. Luhmann et al. 2004; Tóth et al. 2005). However, despite the increased computer power, running a full 3D simulation from Sun to Earth remains very expensive and time consuming. Therefore, 1D models are still fairly popular in space weather research and for solar wind predictions (e.g. Zieger and Hansen 2008; Feng et al. 2009). The 1D polytropic model

presented here runs fast, is easily adjustable to obtain the desired solar wind speed, density, and temperature, and it is straightforward extensible to an axisymmetric solar wind model. Numerical simulations have pointed to the importance of an accurate modelling of the background medium in which CMEs propagate. The density and velocity distribution of the solar wind will influence the shape and velocity of the CME associated shock front (Jacobs et al. 2005; Wu et al. 2005). Observationally driven simulations of the interplanetary propagation of CMEs are indispensable to obtain a correct interpretation of the observations and to get insight in their complex structure and dynamics (Lugaz et al. 2008, 2009). The 2.5D extension of the wind model presented in this paper can serve as a background model for CME initiation and propagation studies under solar minimum conditions. **However, some caution has to be taken when studying shock propagation in polytropic models. As already mentioned before, energy is not conserved in this model and as such the well known Rankine-Hugoniot relations are not longer applicable. However, the same remark is true for every other MHD model using source terms. Moreover, the result of shock propagation in a polytropic model can significantly differ from a full MHD simulation. This has been demonstrated by Pomoell and Vainio (2011), who constructed a polytropic wind model with $\alpha = 1.05 = \gamma$ and an MHD model with $\gamma = 5/3$, including an additional heating term in the energy equation in order to obtain the exact same solution for the steady state wind as in the polytropic case. A CME was launched in both configurations and the clear difference in the compression ratio and in the extend of the shock front can be remarked. As has been noted by van der Holst et al. (2010) the models using a reduced and variable polytropic index do not well-describe CME driven shocks. This is because the value of the polytropic index is kept fixed in time, and as such induces unphysical pressure (and thus temperature) when the solar wind diverges from its stationairy state due to, for example, the passage of a CME.**

Acknowledgments

This research was funded by projects GOA/2009-009 (K.U.Leuven), G.0304.07 (FWO-Vlaanderen), 3E090665 (FWO-Vlaanderen), and C 90347 (ESA Prodex 9). Financial support by the European Commission through the SOLAIRE Network (MTRN-CT-2006-035484) and support from the European Commission's Seventh Framework

Programme (FP7/2007-2013) under the grant nr. 218816 (SOTERIA project) is gratefully acknowledged. For the simulations we used the infrastructure of the VSC - Flemish Supercomputer Center, funded by the Hercules foundation and the Flemish Government - department EWI. We thank the ACE SWEPAM instrument team and the ACE Science Center for providing the ACE data.

References

Breen, A. R., Thomasson, P., Jordan, C. A., Tappin, S. J., Fallows, R. A., Canals, A., Moran, P. J., 2002. Slow and fast solar wind acceleration near solar maximum. Adv. Space. Res. 30 (3), 433–436.

Chandrasekhar, S., 1939. An introduction to the study of stellar structure. Chicago, Ill., The University of Chicago press.

Cohen, O., Sokolov, I. V., Roussev, I. I., Arge, C. N., Manchester, W. B., Gombosi, T. I., Frazin, R. A., Park, H., Butala, M. D., Kamalabadi, F., Velli, M., 2007. A semiempirical magnetohydrodynamical model of the solar wind. ApJ 654, L163–L166.

Cohen, O., Sokolov, I. V., Roussev, I. I., Gombosi, T. I., 2008. Validation of a synoptic solar wind model. J. Geophys. Res 113, A03104.

Ebert, R. W., McComas, D. J., Elliott, H. A., Forsyth, R. J., Gosling, J. T., jan 2009. Bulk properties of the slow and fast solar wind and interplanetary coronal mass ejections measured by Ulysses: Three polar orbits of observations. J. Geophys. Res 114 (A13), 1109.

Evans, C. R., Hawley, J. F., 1988. Simulation of magnetohydrodynamic flows: a constrained transport method. ApJ 332, 659–677.

Feng, X. S., Zhang, Y., Yang, L. P., Wu, S. T., Dryer, M., oct 2009. An operational method for shock arrival time prediction by one-dimensional CESE-HD solar wind model. J. Geophys. Res 114 (A13), 10103.

Fludra, A., Del Zanna, G., Alexander, D., Bromage, B., 1999. Electron density and temperature of the lower solar corona. J. Geophys. Res 104 (A5), 9709–9720.

Goldstein, B. E., Neugebauer, M., Phillips, J. L., Bame, S., Gosling, J. T., McComas, D., Wang, Y., Sheeley, N. R., Suess, S. T., dec 1996. ULYSSES plasma parameters: latitudinal, radial, and temporal variations. A&A 316, 296–303.

Hayashi, K., Benevolenskaya, E., Hoeksema, T., Liu, Y., Zhao, X. P., jan 2006. Three-Dimensional Magnetohydrodynamic Simulation of a Global Solar Corona Using a Temperature Distribution Map Obtained from SOHO EIT Measurements. ApJ 636, L165–L168.

Hollweg, J. V., 1986. Transition region, corona, and solar wind in coronal holes. J. Geophys. Res 91, 4111–4125.

Hu, Y. Q., Feng, X. S., Wu, S. T., Song, W. B., 2008. Three-dimensional MHD modeling of the global corona throughout solar cycle 23. Journal of Geophysical Research (Space Physics) 113 (A12), 3106.

Jacobs, C., Poedts, S., van der Holst, B., Chané, E., 2005. On the effect of the background wind on the evolution of interplanetary shocks. A&A 430, 1099 – 1107.

Keppens, R., Goedbloed, J. P., March 1999. Numerical simulations of stellar winds: polytropic models. A&A 343, 251 – 260.

Keppens, R., Goedbloed, J. P., February 2000. Stellar winds, dead zones, and coronal mass ejections. ApJ 530, 1036 – 1048.

Kojima, M., Breen, A. R., Fujiki, K., Hayashi, K., Ohmi, T., Tokumaru, M., 2004. Fast solar wind after the rapid acceleration. J. Geophys. Res 109, A04103.

Linker, J., Mikić, Z., January 1995. Disruption of a helmet streamer by photospheric shear. ApJ 438, L45 – L48.

Linker, J., Mikić, Z., Biesecker, A., Forsyth, R. J., Gibson, S. E., Lazarus, A. J., Lecinski, A., Riley, P., Szabo, A., Thompson, B. J., May 1999. Magnetohydrodynamic modeling of the solar corona during Whole Sun Month. J. Geophys. Res 104, 9809 – 9830.

Linker, J. A., Mikić, Z., Lionello, R., Riley, P., Amari, T., Odstrcil, D., 2003. Flux cancellation and coronal mass ejections. Phys. Plas. 10 (5), 1971–1978.

Lugaz, N., Vourlidas, A., Roussev, I. I., Jacobs, C., Manchester, IV, W. B., Cohen, O., September 2008. The Brightness of Density Structures at Large Solar Elongation Angles: What Is Being Observed by STEREO SECCHI? ApJ 684, L111–L114.

Lugaz, N., Vourlidas, A., Roussev, I. I., Morgan, H., 2009. Solar Terrestrial Simulation in the STEREO Era: The 24 25 January 2007 Eruptions. Sol. Phys. 256, 269–284.

Luhmann, J. G., Solomon, S. C., Linker, J. A., Lyon, J. G., Mikić, Z., Odstrcil, D., Wang, W., Wiltb erger, M., 2004. Coupled model simulation of a Sun-to-Earth space weather event. J. Atmosph. and Solar-Terrestrial Phys. 66, 1243–1256.

McComas, D. J., Ebert, R. W., Elliott, H. A., Goldstein, B. E., Gosling, J. T., Schwadron, N. A., Skoug, R. M., sep 2008. Weaker solar wind from the polar coronal holes and the whole Sun. Geophys. Res. Lett. 35, 18103.

McComas, D. J., Elliott, H. A., Schwadron, N. A., Gosling, J. T., Skoug, R. M., Goldstein, B. E., 2003. The three-dimensional solar wind around solar maximum. Geophys. Res. Lett. 30 (10), 1517.

McIntosh, S. W., De Pontieu, B., Carlsson, M., Hansteen, V., Boerner, P., Goossens, M., 2011. Alfvénic waves with sufficient energy to power the quiet solar corona and fast solar wind. Nature 475, 477–480.

Nakamizo, A., Tanaka, T., Kubo, Y., Kamei, S., Shimazu, H., Shinagawa, H., jul 2009. Development of the 3-D MHD model of the solar corona-solar wind combining system. J. Geophys. Res 114 (A13), 7109.

Ofman, L., 2010. Wave modeling of the solar wind. Living Rev. Solar Phys. 7.
URL http://www.livingreviews.org/lrsp-2010-4

Parker, E. N., 1958. Dynamics of the interplanetary gas and magnetic fields. ApJ 128, 664 – 676.

Parker, E. N., 2007. Conversations on electric and magnetic fields in the cosmos. Princeton University Press.

Pomoell, J., Vainio, R., 2011. A note on using thermally driven solar wind models in MHD space weather simulations. In: IAU Symposium. Vol. 274 of IAU Symposium. pp. 102–104.

Riley, P., Linker, J. A., Mikić, Z., Lionello, R., Ledvina, S. A., Luhmann, J. G., 2006. A comparison between global solar magnetohydrodynamic and potential field source surface model results. ApJ 653, 1510–1516.

Roussev, I. I., Gombosi, T. I., Sokolov, I. V., Velli, M., Manchester, W. B., DeZeeuw, D. L., Liewer, P., Tóth, G., Luhmann, J., 2003. A three-dimensional model for the solar wind incorporating solar magnetogram observations. ApJ 595, L57 – L60.

Schwenn, R., 2006. Solar wind sources and their variations over the solar cycle. Space. Sc. Rev. 124, 51–76.

Tóth, G., 1996. General Code for Modeling MHD flows on Parallel Computers: Versatile Advection Code. Astrophys. Lett. & Comm. 34, 245.

Tóth, G., Sokolov, I. V., Gombosi, T. I., Chesney, D. R., Clauer, C. R., De Zeeuw, D. L., Hansen, K. C., Kane, K. J., Manchester, W. B., Oehmke, R. C., Powell, K. G., Ridley, A. J., Roussev, I. I., Stout, Q. F., Volberg, O., 2005. Space Weather Modeling Framework: A new tool for the space science community. J. Geophys. Res 110, A12226.

Totten, T. L., Freeman, J., Arya, S., 1995. An empirical determination of the polytropic index for the free-streaming solar wind using Helios 1 data. J. Geophys. Res 100, 13 – 17.

Usmanov, A. V., Goldstein, M. L., 2006. A three-dimensional MHD solar wind model with pickup protons. J. Geophys. Res 111, A07101.

van der Holst, B., Manchester IV, W. B., Frazin, R. A., Vásquez, A. M., Tóth, G., Gombosi, T. I., 2010. A data-driven, two-temperature solar wind model with Alfvén waves. ApJ 725, 1373–1383.

Van Doorsselaere, T., Wardle, N., Del Zanna, G., Jansari, K., Verwichte, E., Nakariakov, V. M., 2011. The first measurement of the adiabatic index in the solar corona using time-dependent scpectroscopy of Hinode/EIS observations. ApJ 727, L32.

Wang, A. H., Wu, S. T., Suess, S. T., Poletto, G., 1995. Numerical modeling of coronal mass ejections based on various pre-event model atmospheres. Sol. Phys. 161, 365–381.

Weber, A. J., Davis, L., 1967. The angular momentum of the solar wind. ApJ 148, 217 – 227.

Wu, C.-C., Fry, C. D., Berdichevsky, D., Dryer, M., Smith, Z., Detman, T., 2005. Predicting the Arrival Time of Shock Passages at Earth. Sol. Phys. 227, 371–386.

Wu, S. T., Guo, W. P., Michels, D. J., Burlaga, L. F., 1999. MHD description of the dynamical relationships between a flux rope, streamer, coronal mass ejection, and magnetic cloud: An analysis of the January 1997 Sun-Earth connection event. J. Geophys. Res 104 (A7), 14789–14801.

Zieger, B., Hansen, K. C., aug 2008. Statistical validation of a solar wind propagation model from 1 to 10 AU. J. Geophys. Res 113 (A12), 8107.

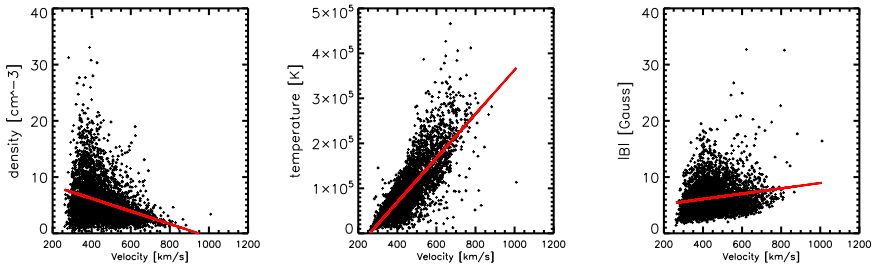

Figure 1: ACE data over the period 1998 – 2008.

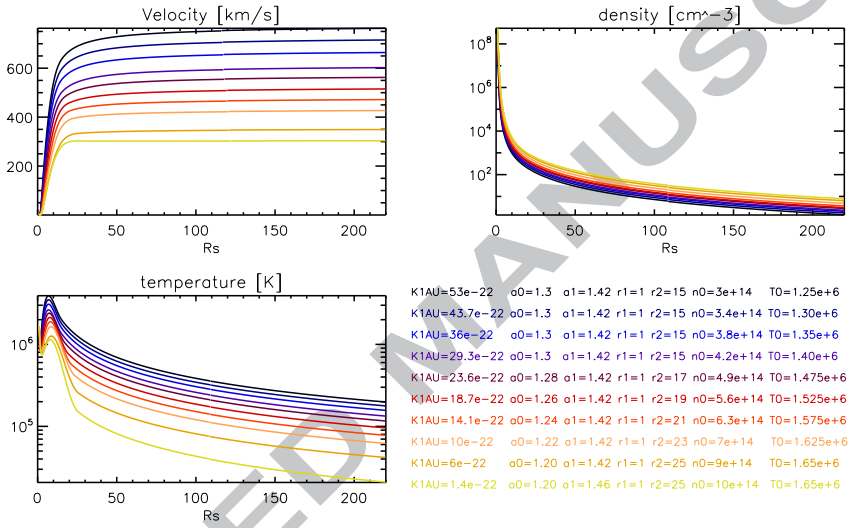

Figure 2: Radial variation of the solar wind variables for the 1.5D simulations listed in Table 1.

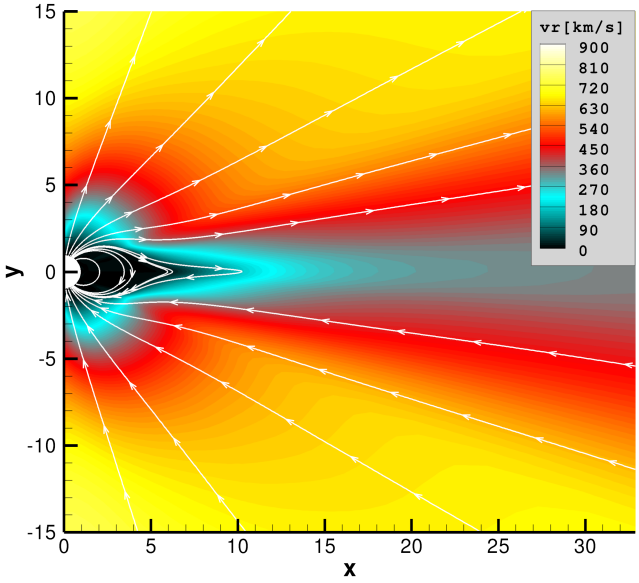

Figure 3: Visualisation of the 2.5D solar wind simulation. The colour code represents radial velocity and the white lines mark magnetic field lines.

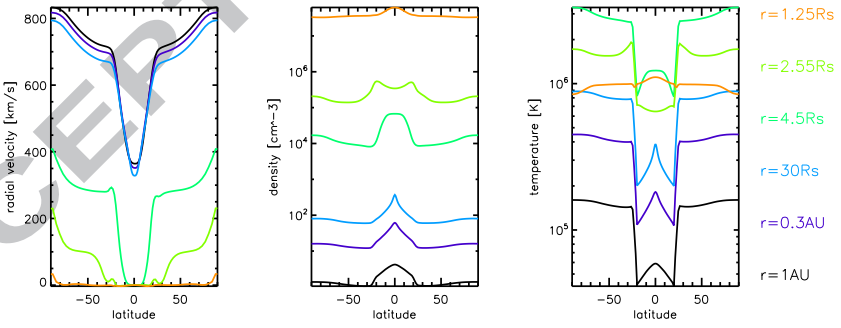

Figure 4: The angular variation of the solar wind velocity, the density, and the temperature obtained from the 2.5D simulation. Different colours represent different radial distances, varying between $1.25R_{\odot}$ and 1AU.

Table 1: Overview of the different 1.5D solar wind simulations. Rows 1 to 3 contain the desired solar wind quantities at 1AU, the different model parameters are listed in rows 4 to 10, and the obtained output is displayed in rows 10 to 12.

V_∞ [km s^{-1}]	750	700	650	600	550	500	450	400	350	300
n^p_{ACE} [cm^{-3}]	2.2	2.8	3.4	3.9	4.5	5.1	5.6	6.2	6.8	7.3
T^p_{ACE} [K]	240 781	216 293	191 805	167 317	142 829	118 341	93 853	69 365	44 877	20 389
$K_{1\mathrm{AU}}$										
[10^{-22}Nm$^{3\alpha-2}$]	53.4	43.7	35.8	29.3	23.6	18.7	14.1	10.0	6.2	1.4
α_0	1.30	1.30	1.30	1.30	1.28	1.26	1.24	1.22	1.20	1.20
α_1	1.42	1.42	1.42	1.42	1.42	1.42	1.42	1.42	1.42	**1.46**
r_1 [$R_\odot$]	1	1	1	1	1	1	1	1	1	1
r_2 [$R_\odot$]	15	15	15	15	17	19	21	23	25	25
n_0 [10^{14}m^{-3}]	3.0	3.4	3.8	4.2	4.9	5.6	6.3	7.0	9.0	10.0
T_0 [10^6K]	1.250	1.300	1.350	1.400	1.475	1.525	1.575	1.625	1.650	1.650
$V_{1\mathrm{AU}}$ [km s^{-1}]	762	714	663	602	561	514	470	426	349	300
$n^p_{1\mathrm{AU}}$ [cm^{-3}]	1.5	1.8	2.2	2.4	2.9	3.2	3.8	5.0	6.6	8.1
$T^p_{1\mathrm{AU}}$ [K]	202 266	181 332	160 185	136 250	118 815	97 850	79 420	63 286	42 650	21 418

Table 2: The radial velocity, the proton density, and the temperature at a radial distance of 0.3AU and 1AU in the simulated solar wind for solar minimum conditions.

	V	n_{p+}	T
		pole	
0.3AU	815 km s^{-1}	16 cm^{-3}	4.49×10^5K
1AU	830 km s^{-1}	1.37 cm^{-3}	1.6×10^5K
		equator	
0.3AU	351 km s^{-1}	60 cm^{-3}	1.81×10^5K
1AU	364 km s^{-1}	4.2 cm^{-3}	5.9×10^4K